Modulated structures in electroconvection in nematic liquid crystals

S. Komineas,[1] H. Zhao,[2] and L. Kramer[1]
[1]*Physikalisches Institut, Universität Bayreuth, D-95440 Bayreuth, Germany*
[2]*Max-Planck-Institut für Physik komplexer Systeme, Nöthnitzer Strasse 38, D-01187 Dresden, Germany*
(Received 26 July 2002; published 10 March 2003)

Motivated by experiments in electroconvection in nematic liquid crystals with homeotropic alignment we study the coupled amplitude equations describing the formation of a stationary roll pattern in the presence of a weakly damped mode that breaks isotropy. The equations can be generalized to describe the planarly aligned case if the orienting effect of the boundaries is small, which can be achieved by a destabilizing magnetic field. The slow mode represents the in-plane director at the center of the cell. The simplest uniform states are normal rolls, which may undergo a pitchfork bifurcation to abnormal rolls with a misaligned in-plane director. We present a new class of defect-free solutions with spatial modulations perpendicular to the rolls. In a parameter range where the zigzag instability is not relevant these solutions are stable attractors, as observed in experiments. We also present two-dimensionally modulated states with and without defects which result from the destabilization of the one-dimensionally modulated structures. Finally, for no (or very small) damping, and away from the rotationally symmetric case, we find static chevrons made up of a periodic arrangement of defect chains (or bands of defects) separating homogeneous regions of oblique rolls with very small amplitude. These states may provide a model for a class of poorly understood stationary structures observed in various highly conducting materials (''prechevrons'' or ''broad domains'').

DOI: 10.1103/PhysRevE.67.031701 PACS number(s): 61.30.Gd, 47.20.Ky, 47.65.+a

I. INTRODUCTION

Nematic liquid crystals, the simplest type of intrinsically anisotropic fluids, continue to provide model systems for a wide variety of interesting nonlinear dynamical phenomena like optical instabilities [1], flow-induced nonlinear waves [2], critical properties of nonequilibrium transitions [3], and in particular electrically or thermally driven convection instabilities [3,4] (see also Ref. [5] and references therein).

In nematics the mean orientation of the rodlike molecules is described by the director $\hat{n}$. Electroconvection (EC) driven by an ac voltage U at frequency ω is commonly observed in thin nematic layers sandwiched between glass plates with transparent electrodes using nematics with positive conductivity anisotropy ($\sigma_a > 0$) and negative or slightly positive dielectric anisotropy ϵ_a. In the well studied *planarly* aligned case, where $\hat{n}$ is anchored parallel to the bounding plates along a direction which we will take as x (we choose the layer in the x-y plane) EC sets in directly from the homogeneous state at a critical voltage $U_c(\omega)$ and leads slightly above threshold to ordered roll patterns associated with a periodic director distortion with the critical wave vector $\vec{q}_c(\omega)$. Here we will only consider the most common situation, where the bifurcation is supercritical and leads to stationary rolls with $\vec{q}_c$ parallel to $\hat{x}$ [normal rolls (NRs)]. In the usual low-frequency conduction regime, where the wavelength is controlled by the cell thickness, this may exclude in particular very low frequencies, where the rolls at threshold may be oriented obliquely (depending on the material). In NRs near threshold the director remains in the x-z plane, i.e., perpendicular to the roll axis.

The investigation of homeotropically oriented cells using nematics with manifestly negative dielectric anisotropy $\epsilon_a < 0$ was initiated rather recently, see Refs. [6–9] for experimental and [10–12] for theoretical work. In this case the director is initially oriented perpendicular to the layer, i.e., in the z direction, so the system is isotropic in the x-y plane. Then the first instability is the spatially homogeneous Fréedericksz transition where the director bends away from the z direction, singling out spontaneously a direction $\hat{c}$ in the x-y plane. After the transition the slow, undamped variation of the in-plane director $\hat{c}$ (the Goldstone mode) may be described by an angle ϕ. At higher voltages there is a further transition to EC, which is in many respects similar to that in cells with planarly aligned nematics. However, now the Goldstone mode has to be included in the description even right at threshold. It turns out that the torque arising when the in-plane director and the wave vector are (slightly) misaligned is destabilizing, i.e., it acts to increase the misalignment (''abnormal torque''). Then the in-plane director in NRs is not perpendicular to the (local) roll axis. These NRs with a misaligned in-plane director were termed abnormal rolls (ARs) [6]. Furthermore one may expect spatiotemporal disorder right at threshold and this has indeed been observed, at least in the oblique roll regime, where one expects faster dynamics [9,11,13]. For NRs the experimental situation is not totally clear [13].

By applying an in-plane magnetic field, which now defines the x direction and exerts an aligning torque on $\hat{c}$, the disorder at threshold can be suppressed. Indeed the situation then is similar to that in the planar case. However, for a small field a small abnormal torque will suffice to overcome the magnetic alignment, and then one has a transition to ordered ARs, where the in-plane director is homogeneously rotated out of the x direction. For NRs this symmetry breaking is spontaneous, either to the left or to the right, and the transition is described by a supercritical pitchfork bifurcation, which has been verified experimentally [14,15].

In the planarly aligned case one also has a transition to ordered ARs, although this occurs at a distance from threshold such that a quantitative description is more difficult. Since now the director is aligned at the cell boundaries the distortion of the in-plane director is confined to the center part of the cell leading to a twist distortion. Incidentally, this is the reason why the phenomenon has been identified only recently in planar convection [16]. By applying a magnetic field in the y direction one can now destabilize $\hat{c}$ and thus move the AR transition downward towards the primary instability. The AR transition merges with the primary bifurcation when the field reaches the strength of the twist Freedericksz field. When the two transitions are near each other a simple reduced description can be used. This shows that the two classes of systems are similar in many ways.

Above the AR transition one often observes more complicated structures with or without defects. In particular, in homeotropic EC, modulations of the AR mode have been observed which leave the roll pattern (i.e., its phase) virtually unchanged [14,15]. Ideally, such structures can be considered quasi one dimensional (1D) with spatial variations only perpendicular to the (normally oriented) rolls. We wish to address in particular such structures by studying the simplest set of coupled amplitude equations capable of describing the AR scenario. These equations were first derived for homeotropic systems near threshold [11,17] but with a slight generalization they can also illustrate the planar case. We present here 1D solutions of the appropriate type. We will then briefly discuss the destabilization of these 1D structures. Finally we present a new class of fully ordered 2D solutions occurring at higher voltage (or smaller magnetic fields) involving periodic arrangements of defect chains (or bands of defects). We call them static chevrons since they are reminiscent of the dynamic chevrons observed in the dielectric range of EC, and more recently, also in homeotropic convection [13].

Our results could also be of relevance for the higher-frequency dielectric regime, where the rolls are very narrow and therefore the orienting effect of planar boundary conditions is substantially weaker than in the conduction range. Recently, the weakly nonlinear description of the dielectric regime in planarly aligned systems has been investigated in detail [18].

In Sec. II we discuss the basic equations, which take the form of an activator-inhibitor system, and their homogeneous solutions. In Sec. III we study 1D modulated solutions. Their stability within the full 2D equations is investigated in Sec. IV A and in Sec. IV B some 2D structures, in particular defect-free solutions, are presented. In Sec. V we present the static chevron states. We conclude by putting our results into a more general context, relate them to experiments, and present an outlook.

II. BASIC EQUATIONS AND HOMOGENEOUS SOLUTIONS

In situations where the in-plane director, described by an angle φ measured from the x direction, becomes an active mode already near the threshold to NRs one can describe the system by the following set of coupled Ginzburg-Landau equations for the complex patterning mode A and the slowly varying angle φ [11,17]:

$$\check{\tau}\partial_{\check{t}}\check{A}=[\varepsilon+\xi_{xx}^2\partial_{\check{x}}^2+\xi_{yy}^2(\partial_{\check{y}}^2-2iq_cC_1\varphi\partial_{\check{y}}-C_2\varphi^2)-g|\check{A}|^2+i\check{\nu}\partial_{\check{y}}\varphi]\check{A}, \tag{1}$$

$$\check{\gamma}_1\partial_{\check{t}}\varphi=K_1\partial_{\check{y}}^2\varphi+K_3\partial_{\check{x}}^2\varphi-T\varphi+\frac{\Gamma}{4}[-iq_c\check{A}^*(\partial_{\check{y}}-iq_c\varphi)\check{A}+\text{c.c.}]. \tag{2}$$

Here we have chosen the x direction along the wave vector of the NRs. The angle φ of the in-plane director is measured from the x axis. The validity of Eqs. (1) and (2) is restricted to small values of the reduced control parameter (more precisely $\varepsilon/g\ll 1$ and angles $|\varphi|\ll 1$). Special attention should be paid to the sign of the parameter Γ. If Γ were positive the field φ would be stabilized by the roll pattern. However, Γ is negative, at least for the standard nematics which have been used in relevant experiments [11,17,18]. This gives rise to the transition to abnormal rolls and to interesting dynamical phenomena. Note that ξ_{yy} tends to zero at the transition from normal to oblique rolls at threshold.

The equations can be justified most convincingly for homeotropic orientation near the EC threshold (reduced control parameter $\varepsilon\ll 1$). Overall rotation invariance then requires that the three terms multiplying ξ_{yy}^2 in Eq. (1) combine to $(\partial_{\check{y}}-iq_c\varphi)^2$, so that $C_1=C_2=1$. Without the isotropy-breaking term $-T\varphi$, which is realized easily by an in-plane magnetic field (then $T=\check{\chi}_aH^2$), the angle φ may not saturate. Then one has to resort to a globally rotational invariant generalization of Eqs. (1) and (2) [17,11]. We will see that this is not always necessary.

The parameters C_1, C_2 were introduced to allow for more general situations like in planar alignment (for structural stability one needs $C_2>C_1^2>0$). Then the magnetic field term in Eq. (2) actually models the orienting effect of the boundaries. In the common conduction range, where the wavelength is of the order of the cell thickness, the orienting effects are sufficiently strong so that interesting dynamics of φ sets in at values of ε which are too large to allow quantitative description by Eqs. (1) and (2). Then, in particular, singular mean flow has to be included [19,20]. To reduce the damping of φ one can either apply a destabilizing in-plane magnetic field and/or go to the dielectric range, where the effect of boundaries is weaker [18]. When T becomes too small higher-order terms are needed in Eq. (2).

For calculations it is useful to introduce a scaled version of Eqs. (1) and (2) for $\varepsilon>0$,

$$\tau\partial_tA=[1+\partial_x^2+\partial_y^2-2ic_1\phi\partial_y-\phi^2-|A|^2-i\nu\partial_y\phi]A, \tag{3}$$

$$\partial_t\phi=D_1\partial_x^2\phi+D_2\partial_y^2\phi-h\phi+\left[\frac{i}{2}A^*(c_2\partial_y-i\phi)A+\text{c.c.}\right], \tag{4}$$

where

$$\check{A}=(\varepsilon/g)^{1/2}A, \quad \varphi=\varepsilon^{1/2}\phi/(\xi_{yy}q_c\sqrt{C_2}),$$

$$\check{x}=\xi_{xx}\varepsilon^{-1/2}x, \quad \check{y}=\xi_{yy}\varepsilon^{-1/2}y, \quad \check{t}=2\check{\gamma}_1 g t/(\varepsilon|\Gamma|q_c^2),$$

$$\tau=\check{\tau}|\Gamma|q_c^2/(2\check{\gamma}_1 g), \quad \nu=\check{\nu}/(\xi_{yy}^2 q_c\sqrt{C_2}),$$

$$D_1=2K_3 g/(|\Gamma|q_c^2\xi_{xx}^2), \quad D_2=2K_1 g/(|\Gamma|q_c^2\xi_{yy}^2),$$

$$c_1=C_1/\sqrt{C_2}, \quad c_2=\sqrt{C_2}, \quad h=2Tg/(|\Gamma|q_c^2\varepsilon). \tag{5}$$

The damping parameter h gives the ratio of the aligning (=isotropy breaking) torque over the abnormal torque of NRs. For large values of h one can set $\phi=0$ and disregard Eq. (4). h can be decreased by either decreasing a stabilizing magnetic field (increasing a destabilizing field) or by increasing ε. Below we will show that, keeping the aligning torque fixed, one can write

$$h=\varepsilon_{\mathrm{AR}}/\varepsilon, \tag{6}$$

where $\varepsilon_{\mathrm{AR}}$ is the reduced control parameter, where the transition from NRs to ARs takes place. The parameter ν describes the action of the gradient of the in-plane director on the phase of the rolls. Experimentally it can be controlled by varying the frequency. In this paper, we will be concerned with the range $\nu>0$, where NRs are first destabilized by the transition to ARs (see below). For $\nu<0$ the zigzag instability comes in earlier. Various features of Eqs. (3) and (4) have been analyzed in Refs. [11,17,21] and comparison with experiment has given evidence for their validity.

We first discuss the homogenous solutions of Eqs. (3) and (4) for rolls with modulation wave vector (Q,P) where $A=A_0e^{i(Qx+Py)}$, $A_0\geqslant 0$, and a constant in space angle $\phi=\phi_0$. One is left with the dynamical system

$$\tau\partial_t A_0=[1-Q^2-P^2+2c_1P\phi_0-\phi_0^2-A_0^2]A_0,$$

$$\partial_t\phi_0=(A_0^2-h)\phi_0-c_2PA_0^2. \tag{7}$$

These equations can be classified as an activator-inhibitor system with activator A_0 (positive linear growth rate for not too large wave vector) and inhibitor ϕ_0. For simplicity we will in the following consider $Q=0$ (the results are easily generalized). For $P=0$ (rolls exactly in the x direction; we will deal with this case, except in Sec. V) there is the symmetry $\phi\rightarrow-\phi$. The basic uniform state $A_0=0$, $\phi_0=0$, is an unstable solution of Eq. (7), and the NR state $A_0=1$, $\phi_0=0$, is stable only for $h\geqslant 1$. Finally, the abnormal roll (AR) states

$$A_{\mathrm{AR}}=\sqrt{h}, \quad \phi_{\mathrm{AR}}=\pm\sqrt{1-h} \tag{8}$$

exist in the range $0\leqslant h<1$. They bifurcate from the NRs at $h=1$ and they break the symmetry $\phi\rightarrow-\phi$ of the equations. For $h>0$ the two AR states are global attractors with regions of attraction $A_0>0$, $\phi_0>$ or <0, respectively. For $h>4\tau/(1+4\tau)$ the AR states represent saddles (two real eigenvalues), otherwise spiral points.

The case $h=0$ needs special attention. Clearly the whole band

$$A_0=0, \quad \phi_0=\mathrm{const} \tag{9}$$

is the solution of the equation. The segment $|\phi_0|<1$ is repulsive, whereas the regions $|\phi_0|>1$ are attractive. The AR state (for $h=0$) separates the two cases. There is a separatrix $A_0^2+1/(1+\tau)\phi_0^2=1$, which separates trajectories flowing out of the repulsive segment from those coming from infinity.

The degeneracy for $h=0$ is presumably realistic for homeotropic EC. It is a consequence of rotational invariance. For planar EC the degeneracy is removed by higher-order terms, in particular a term proportional to ϕ^3 in Eq. (4). Nevertheless it is instructive to study this limit where results simplify.

III. 1D MODULATED STRUCTURES

Next we consider modulated structures that leave the roll pattern untouched, i.e., which do not involve the phase of the complex field A. This can occur generically only for spatial variations along x. Then the equations take the form

$$\tau\partial_t A=(\partial_x^2+1-A^2-\phi^2)A, \tag{10}$$

$$\partial_t\phi=(D_1\partial_x^2+A^2-h)\phi. \tag{11}$$

In this section we will study these equations. We will choose $A>0$.

A. Single domain walls

We start by discussing domain walls that connect the two variants of AR solutions and their interaction. Near the AR transition (h near 1) domain walls attract each other, so that modulated states are unstable. This can be seen from the fact that for $1-h\ll 1$ the amplitude can be eliminated adiabatically from Eq. (10) leading to

$$\partial_t\phi=(D_1\partial_x^2+1-h-\phi^2)\phi. \tag{12}$$

In this equation all modulated states (they can be expressed in terms of an elliptic integral) are unstable, although their lifetimes are exceedingly long due to the exponentially weak (attractive) interaction between well separated domain walls (see below).

Surprisingly, for lower damping, the interaction acquires repulsive parts, so that stable modulated structures can emerge. In fact, for $h\rightarrow 0$ the interaction becomes purely repulsive so that only *periodic* modulations exist (see below).

Actually, for $h=0$ a static domain wall solution can be found analytically. It reads

$$A_w(x)=A_0\,\mathrm{sech}(\beta x), \quad \phi_w(x)=\phi_0\tanh(\beta x), \tag{13}$$

where

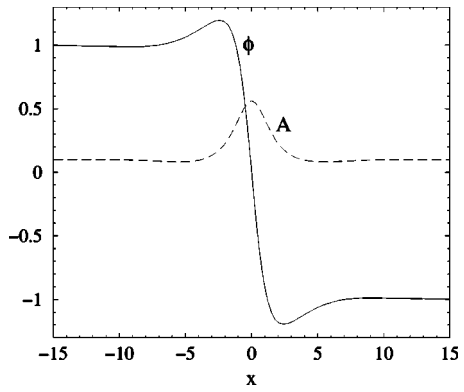

FIG. 1. Domain wall solution connecting the two abnormal roll states $A=h$, $\phi=\pm\sqrt{1-h}$ for $D_1=0.2$ and $h=0.01$.

$$\beta^2=\frac{1}{1+2D_1},\quad A_0^2=2D_1\beta^2,\quad \phi_0^2=2(1+D_1)\beta^2. \tag{14}$$

It selects the states $A=A_0,\phi=\pm\phi_0$ from the continuum of states (9). We have checked numerically and could find no stable static domain wall solution other than Eq. (13). We note that since $\phi_0^2>1$ Eq. (13) connects stable states.

We mention that stationary wall (13) is embedded in a continuous family of moving walls connecting inequivalent states (9). Their study is beyond the scopes of the present paper.

Since for $h\neq 0$ the walls can connect only to the AR states and $\phi_{\rm AR}\to\pm 1$ $(\neq\phi_0)$ for $h\to 0$, this limit has to be clarified. An example of a numerically stable (within the 1D equations) wall for small h is shown in Fig. 1. The fields go to their AR values at spatial infinity. However, in the wall region the field ϕ exhibits an overshoot approaching the values $\pm\phi_0$ of Eq. (13). The overshoot becomes longer and approaches nearer to $\pm\phi_0$ as $h\to 0$.

In order to understand this behavior better, we study the spatial decay of the solution into the AR state. This is obtained by linearizing Eqs. (10) and (11) around an AR solution and calculating the spatial exponents. They are

$$p_\pm^2=h\pm\sqrt{h^2-\frac{4h(1-h)}{D_1}}. \tag{15}$$

For $h\to 0$ the exponents are complex and tend to zero, which explains the slow decay. The exponents $p_\pm$ remain complex for damping constants $h<h_{\rm osc}\equiv(1+D_1/4)^{-1}$. We will show that this is the bound up to which domain walls may repel and thus form stable bound states.

B. Interaction of domain walls, modulated structures

In simulations of Eqs. (10) and (11) one easily finds stable stationary solutions with more than one domain wall. In particular there are periodic solutions which come in two varieties: those that preserve the global symmetry $\phi\to-\phi$ (symmetric) and others that do not preserve it (nonsymmetric). This section is mainly devoted to periodic solutions. There are also pulse-type states localized around one of the AR solutions as well as nonperiodic extended solutions.

Let us first approach these modulated solutions from the side of large separation between domain walls by studying their interaction. Repulsive interaction is a prerequisite to form stable periodic states and interaction of both signs are necessary to form nonperiodic arrays [22]. The problem is formulated as follows. Two walls are placed symmetrically around the origin at positions $\pm x_0$. Then the fields have zero derivative at $x=0$. We now focus on the region $x>0$, write the amplitude and angle as $A=A_w[x-x_0(t)]+a[x-x_0(t),t]$, $\phi=\phi_w[x-x_0(t)]+\varphi[x-x_0(t),t]$ and substitute these expressions into Eqs. (10) and (11). In the spirit of small variations *and* slow (slaved) dynamics we keep the terms linear in a and φ, but neglect those that are small and contain time derivatives

$$\dot{x}_0\tau A_w'=-(\partial_x^2+1-3A_w^2-\phi_w^2)a+2A_w\phi_w\varphi,$$
$$\dot{x}_0\phi_w'=-2A_w\phi_w a-(D_1\partial_x^2+A_w-h)\varphi, \tag{16}$$

where the dot denotes time derivatives and the argument of all functions is $x-x_0$.

To satisfy the boundary conditions one needs $a=A_w-A_\infty, a'=-A_w'$ and $\varphi=\phi_w-\phi_\infty,\varphi'=-\phi_w'$ at $x=0$. At the other end $x\to\infty$ the perturbations a and φ should vanish. Multiplying Eq. (16) by the adjoint of the translational mode $(A_w',-\phi_w')$ and integrating from zero to infinity, we obtain an equation that has, on the right-hand side, only the boundary terms at $x=0$. On the left-hand side, the integrals may be extended to $-\infty$ with negligible error leading to

$$(\langle\phi_w'^2\rangle-\tau\langle A_w'^2\rangle)\dot{x}_0=A_w'^2+A_w''(A_w-A_\infty)-D_1[\phi_w'^2+\phi_w''(\phi_w-\phi_\infty)], \tag{17}$$

where $\langle\cdots\rangle\equiv\int_{-\infty}^{\infty}dx\cdots$. This formula can be used only when the term in brackets on the left-hand side is positive, i.e., for

$$\tau<\tau_{accel}\equiv\langle\phi_w'^2\rangle/\langle A_w'^2\rangle. \tag{18}$$

Otherwise translation becomes an active mode, i.e., one expects spontaneous acceleration of the domain wall. This can be shown by retaining the small time derivative terms omitted in Eqs. (16). We will here assume Eq. (18) to hold (experimentally this appears to be the case) and comment briefly on the acceleration instability at the end of this section.

In the special case $h=0$ and for wall (13), expression (17) can be evaluated leading to

$$[2(1+D_1)-\tau D_1]\dot{x}_0=12D_1\beta e^{-2\beta x_0}. \tag{19}$$

Thus, at least for $\tau<\tau_{\rm accel}$ one has $\dot{x}_0>0$, i.e., the interaction among walls is repulsive everywhere. This is consistent with the numerical observation of stable periodic solutions and no nonperiodic states.

For $h\neq 0$, we may use the asymptotic behavior characterized by the exponents in Eq. (15) to evaluate the right-hand

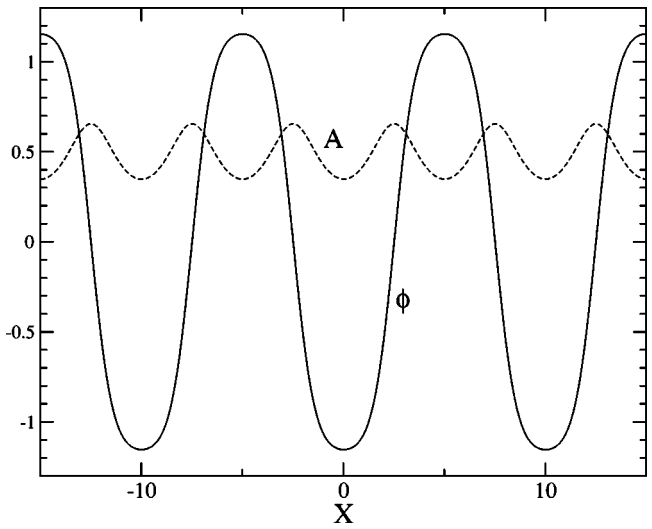

FIG. 2. A symmetric periodic solution for $D_1=0.2$ and $h=0.1$. The dashed line gives the field A and the solid line the field ϕ. It is found by numerical simulation of Eqs. (10) and (11) with periodic boundary conditions.

side of Eq. (17). In the range of complex exponents $p_{\pm}$, i.e., for $h<h_{\rm osc}$, the interaction is repulsive or attractive depending on the distance between walls. Thus one expects stable periodic solutions in appropriate wavelength intervals as well as nonperiodic structures, in agreement with simulations. An example of a periodic solution is given in Fig. 2 for a field value $h=0.1$.

Finally, in the monotonic range $h_{\rm osc}<h<1$, the right-hand side of Eq. (17) is

$$c^2\left[\frac{D_1 p_-^4}{4h(1-h)}-1\right]\exp(2p_- x_0), \tag{20}$$

where c is a factor that cannot be determined from the asymptotic analysis and p_- is given in Eq. (15). One easily sees that the term in square brackets is negative, so that the interaction between domain walls is now attractive. In this range we expect neither stable periodic nor nonperiodic solutions, although, as pointed out before, the lifetime of modulations may be very long.

Let us now continue the symmetric periodic solutions to small wavelengths. Since they conserve the global $\phi\rightarrow-\phi$ symmetry one expects them to bifurcate from the NRs. This is indeed the case. From a simple linear stability analysis one finds that NRs are unstable with respect to periodic modes with wave number $|q|<q_c$, where

$$q_c(h)=\sqrt{\frac{1-h}{D_1}}. \tag{21}$$

Indeed, the bifurcation is of supercritical type. In Fig. 3, which summarizes our results on symmetric periodic solutions, the minimum period $L_{\rm min}=2\pi/q_c(h)$ is shown (dotted curve).

When the (symmetric) periodic solutions are born they inherit the instability of the NRs with respect to symmetry

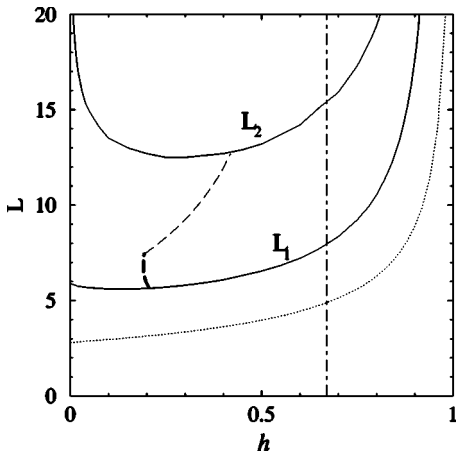

FIG. 3. Stability limits of the symmetric periodic solutions in the period ($=L$) vs the h plane for $D_1=0.2$. Below the line L_1 they are unstable against breaking the $\phi\rightarrow-\phi$ symmetry, leading to ARs. Above the line L_2 they are unstable against a symmetry-broken periodic solution. The dotted line gives the minimum period $L_{\rm min}=2\pi\sqrt{D_1/(1-h)}$, where the periodic solutions bifurcate from NRs. On crossing the dashed line there is a zigzag instability that is either short wave (thin dashed) or long wave (thick dashed). The dash-dotted line is the limit of stability for the ARs.

breaking. For a fixed h and by increasing the period we find that they are stabilized at some period $L_1(h)$. The curve $L_1(h)$ can be calculated by a linear stability analysis. It diverges to infinity for $h\rightarrow h_{\rm osc}$ since above this value no stable periodic solutions are expected to exist according to the asymptotic analysis given earlier. At $L_1(h)$ a branch of unstable periodic solutions with broken $\phi\rightarrow-\phi$ symmetry bifurcates from the symmetric periodic solutions. We find that the symmetric periodic solutions lose stability (for the first time) at $L_2(h)$ in Fig. 3 and from here on one has a stable nonsymmetric periodic solution, where long and short domains alternate. An example for such a solution is shown in Fig. 4 for $h=0.1$. Clearly this is the result of the nonmonotonic behavior of the interaction between domain walls. Presumably the curve $L_2(h)$ also diverges at $h_{\rm osc}$.

An example of a more complicated nonperiodic solution is shown in Fig. 5. Such states have been also observed in

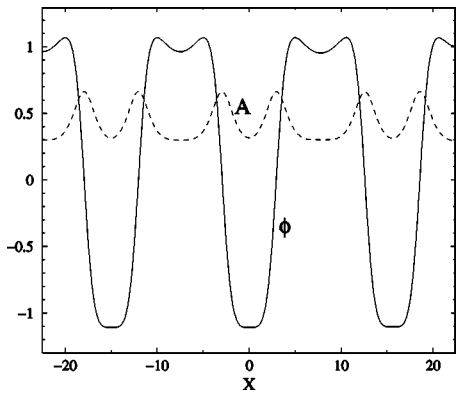

FIG. 4. A nonsymmetric periodic solution for $D_1=0.2$ and $h=0.1$. The dashed line gives the field A and the solid line the field ϕ.

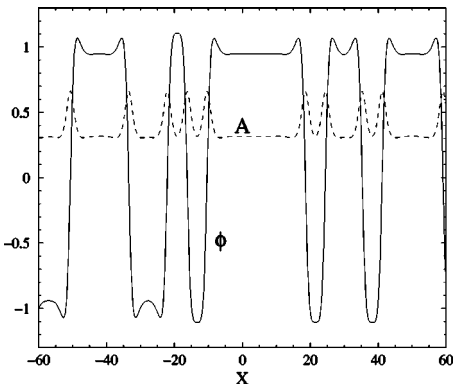

FIG. 5. A nonperiodic solution for $D_1=0.2$ and $h=0.1$. The dashed line gives the field A and the solid line the field ϕ.

Ref. [22]. There is no definite distance between the walls and there seems to be no repeated structure. The state can be spatially chaotic.

Equation (17) indicates that $\dot{x}_0$ diverges at $\tau=\tau_{\rm accel}$. For $h=0$ one finds from Eq. (19)

$$\tau_{\rm accel}=\frac{2(1+D_1)}{D_1}. \tag{22}$$

Computer simulations show that the static wall is unstable, for $\tau\geqslant\tau_{\rm accel}$, to a steadily traveling wall. One sees that on crossing the value $\tau_{\rm accel}$ the wall is accelerated while the direction of motion is spontaneously chosen [23]. No further study of moving walls will be given in this paper. We find numerically that $\tau_{\rm accel}$, as calculated from Eq. (18), increases with h [$\tau_{\rm accel}(h=0)=12, \tau_{\rm accel}(h=0.1)\simeq 16.6, \tau_{\rm accel}(h=0.5)\simeq 26.6$ for $D_1=0.2$]. One could see this also by inspecting the form of the walls.

IV. 2D SOLUTIONS

A. Stability of 1D modulations in the plane

In view of the experimental observation of periodic modulations it is essential to study the stability of the solutions discussed in the preceding section in the context of the full Eqs. (3) and (4) in two dimensions. In order to reduce the number of parameters we will, in this section, consider the case $c_1=c_2=1$ appropriate for homeotropic systems. Some results on the case when c_1 is smaller than 1 will be given in the following section.

For AR solution (8) one can go through a standard linear stability analysis, which gives in the long wavelength limit that, for $\nu>0$, ARs become unstable against zigzag perturbations at $h=2/3$ [11,17,21]. We should also recall that ARs are born from NRs as a stable state at $h=1$, which means that they exist stably for

$$h_{\rm AR}\equiv\frac{2}{3}\leqslant h<1. \tag{23}$$

The value $h_{\rm AR}$ is denoted by a dash-dotted line in Fig. 3. We use in this paper parameter values typical for the standard substance MBBA. Specifically we take [17]

$$D_1=0.2, \quad D_2=0.5, \quad \tau=0.5, \quad \nu=0.6. \tag{24}$$

The positive value for ν indicates that we deal with frequencies above the codimension-2 point, where the zigzag instability of NRs is not operative [11,16,17,24,25].

In order to check the stability of the symmetric periodic solutions found in the preceding section against two-dimensional perturbations we have performed a numerical Floquet analysis. Thus we write the perturbations a,φ of a periodic solution $A_L(x),\phi_L(x)$ with period L as

$$a(x,y,t)=e^{\sigma t+is_y y}\sum_{n=-\infty}^{\infty} a_n \exp(i2\pi nx/L), \tag{25}$$

$$\varphi(x,y,t)=e^{\sigma t+is_y y}\sum_{n=-\infty}^{\infty} \varphi_n \exp(i2\pi nx/L), \tag{26}$$

where a_n,φ_n are constants. We linearize Eqs. (3) and (4) in the perturbations and expand the coefficient functions in the linearized equation, which have the periodicity L, also in a Fourier series. After truncation a system of linear equations is obtained, which can be solved numerically to give the growth rate $\sigma_i(s_y)$ for the linear mode with wave vector s_y. The index i runs over the number of Fourier modes used. The number of modes necessary to achieve a prescribed accuracy is found easily by numerical experimentation.

We have focused on periods which lie between the limits L_1 and L_2 in Fig. 3, i.e., to solutions that are stable with respect to x perturbations. For parameter values (24) our results are included in Fig. 3 (dashed line). The thin dashes (for $7.5\lesssim L\lesssim 13$) indicate a short wave instability of the corresponding period when crossing the line to the left. The thick dashes (for $5.7\lesssim L\lesssim 7.5$) indicate a long wave instability. It is most interesting that the present instabilities occur for a value of h considerably smaller than $h_{\rm AR}$, which means that there are stable periodic solutions for values of h for which the ARs are unstable.

We give the numerical values for the stability limits and the wave vector s_y of the unstable mode for some periodic solutions that we typically use in the simulations of this section (they fit into our typical system length of 64):

$$\begin{aligned} \text{period } 8: &\quad 0.23<h<0.67, \quad s_y=0.67,\\ \text{period } 9.14: &\quad 0.30<h<0.74, \quad s_y=0.69,\\ \text{period } 12.8: &\quad 0.42<h<0.85, \quad s_y=0.66. \end{aligned} \tag{27}$$

The lower limit corresponds to the short wave instability along the y direction with wave vector s_y. The upper limit is due to the instability along the x direction (curve L_1 in Fig. 3).

We conclude that by decreasing the parameter h (which corresponds to increasing the voltage or decreasing the magnetic field in a relevant experiment) below $h_{\rm AR}$ the ARs become unstable but periodic states with certain periods remain stable. They are then expected to be observable under appropriate experimental conditions. As an example we quote the

experiments of Ref. [14] for which the appropriate parameter values are close to Eq. (24) that we use throughout this section. It is reported that for a control parameter corresponding to $h=0.4$ in our theory, periodic modulations of the director orientation are observed. Indeed this value falls into the range where ARs are unstable but some periodic states are expected to be stable. Concerning the periodicity, the tendency towards shorter wavelengths with increasing voltage reported in Ref. [14] is consistent with our results.

B. 2D modulated structures

We now proceed to investigate how the system evolves once the periodic states are destabilized at small values of h, that is, once we cross to the left of the dashed line in Fig. 3. For this purpose we have used a pseudospectral algorithm that simulates the time evolution of Eqs. (3) and (4), which we describe briefly in the following. The linear part of the equation is tranformed into Fourier space and the analytic formula for its time evolution is implemented in the algorithm. For the nonlinear part we work in real space and integrate it in time using a variation of the Euler method. We use periodic boundary conditions in both space dimensions, which are practically enforced by the use of Fourier modes. We typically use 128×128 modes in the two space directions while our physical space has dimensions 64×64 units. Due to the special treatment of the linear part, pseudospectral algorithms allow for a relatively large time step. We typically take $\delta t=0.05$ when we use parameter values (24).

We start a simulation of Eqs. (3) and (4) with a state that is periodic in x, e.g., with period 9.14. The state is stable in the parameter range given in Eq. (27). When we reduce the field h slightly below the value 0.30, we find that the pattern is destabilized and modulations along the y direction appear. The pattern becomes periodic in both spatial dimensions. We give an example of such a state in Figs. 6 and 7, where the fields $|A|$ and ϕ are shown, respectively. The state describes modulations in 2D and has no defects. It was obtained for $h=0.28$. We note that the state in Figs. 6 and 7 is not fully static. It persist for a long time but it is eventually modified through the creation of defects. The system presents persistent dynamics until the end of our simulation, nevertheless, the 2D correlations are preserved to a large extent.

In general, the 2D modulated states reached slightly below the destabilization of 1D periodic modulations are delicate and we have not been able to find a truly static one. The near-periodicity of the final states in both spatial directions is readily seen in the figures resulting from our simulations.

An interesting point is that the defects that are typically created in these processes also show strong 2D correlations. In fact a slightly disordered defect lattice is the usual outcome of such numerical simulations. An example of a reasonably developed defect lattice is presented in Fig. 8 through the field $|A|$. It was obtained by starting the simulation with a periodic state with period 9.14. We used the value $h=0.27$ and the other parameters as in Eq. (24). The initial 1D periodic state is then unstable and evolves into the defect lattice. The time evolution shows that the state has some substantial dynamics but it always remains close to the picture of Fig. 8. Finally, in Fig. 9 we give the ϕ field of the defect lattice of Fig. 8. The ϕ field is predominantly varying in the x direction with small modulations in y.

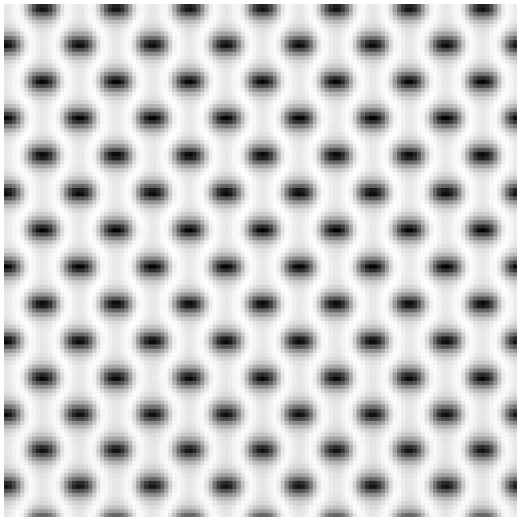

FIG. 6. A two-dimensional periodically modulated pattern without defects from a simulation of Eqs. (3) and (4) for the parameter values (24), $c_1=c_2=1$, and $h=0.28$. Initial conditions: a slightly perturbed periodic modulation state with period 9.14. Shown is a gray-scale representation of the field $|A|$. White corresponds to the maximum value ($|A|=0.85$) and black corresponds to the minimum ($|A|=0.12$). The physical dimensions of the space are 64×64 and we have used periodic boundary conditions.

On further reducing the parameter h the resulting pattern becomes progressively more disordered. A defect chaotic state is eventually obtained for small values of the parameter. In Fig. 10 we show such a state for $h=0.1$. These defect-chaotic states deserve to be studied on their own right but a full investigation of this problem is beyond the scopes of the present paper.

It is not easy to predict in what way the states that we study here would appear in an experiment. Details of the

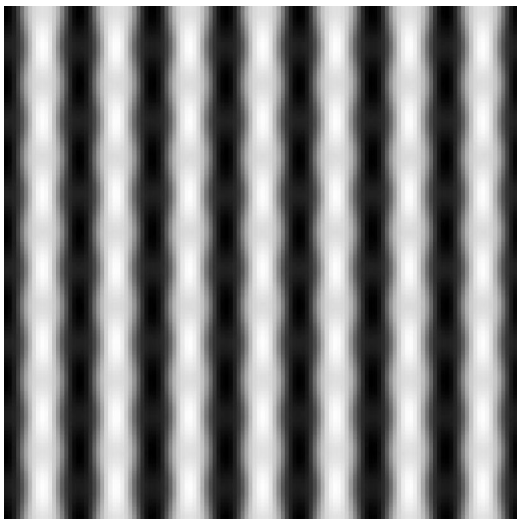

FIG. 7. The field ϕ for the state of Fig. 6. White corresponds to the maximum value and black corresponds to the minimum value ($\phi_m=\pm0.998$).

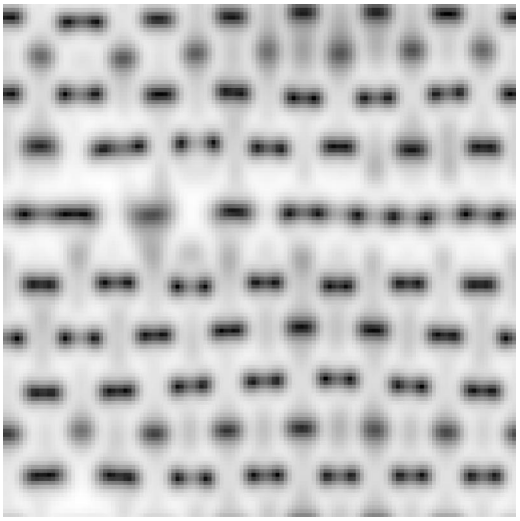

FIG. 8. A reasonably developed defect lattice from simulations of Eqs. (3) and (4) for the parameter values (24), $c_1=c_2=1$, and $h=0.27$. Initial conditions: a slightly perturbed periodic modulation state with period 9.14. Shown is a gray-scale representation of $|A|$. White corresponds to the maximum value and black corresponds to the minimum ($|A|=0$). The state is dynamic but always remains close to that shown. The physical dimensions of our space are 64×64 and we have used periodic boundary conditions.

experimental procedure could be important and the final result can be complicated as is indicated, e.g., by Fig. 7 in Ref. [14], where roughly periodic states without defects are found. In order to observe defect lattices in homeotropic cells, one should remain at small values of ε so that the director angle does not become very large. Otherwise a transition to CRAZY rolls occurs first, which entails formation of disclinations in the director field [15,14]. Also, at higher values of ε, mean-flow effects not included in our simple description become important.

Let us describe the protocol of a numerical simulation, which may give some guidance for experiments. The simulations are performed on a 64×64 domain. We start at a field h above h_{AR} ($h=0.7$) with small spatially random initial conditions of the fields A,ϕ. Experimentally this corresponds to jumping from below the EC threshold directly into the region of stable ARs. Typically, large domains with both AR states appear, separated by walls in the x direction. We then jump to $h=0.4$, where ARs are destabilized while defects are created and a state with 2D correlations sets in. The final state is roughly periodic with period 12.8 in the x direction (5 periods in the domain) and 16 in the y direction (4 periods in the domain). The defects are also roughly ordered in a lattice. After this we increase h gradually in steps of $\delta h=0.02$ and let the system relax in every step for 1000 time units. Although the system never relaxes to a static state, we observe clearly correlations in both spatial directions with the defects approximately ordered in arrays until $h=0.44$ is reached. For $h\geqslant0.46$ the defects annihilate and the system relaxes to a static 1D periodic state with period 12.8. The process described above seems robust in our simulations. Note the interesting fact that there is a range of stable coexistence of the fully ordered 1D state (it is stable down to $h=0.42$) and the 2D solution.

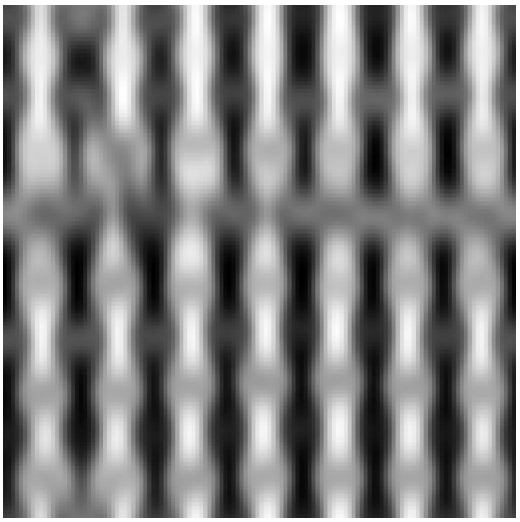

FIG. 9. The field ϕ for the state of Fig. 8. White corresponds to the maximum value and black corresponds to the minimum value.

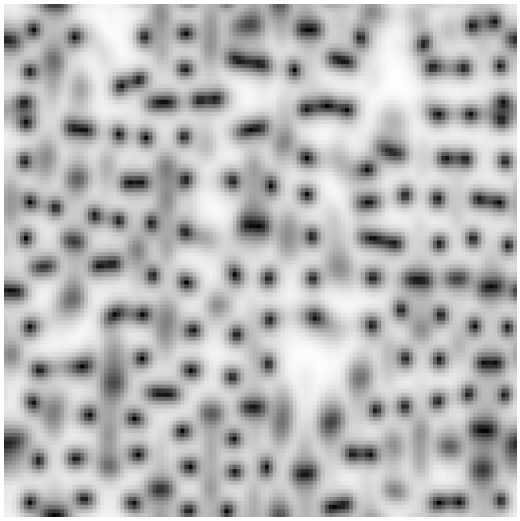

FIG. 10. A disordered state: gray-scale representation of the field $|A|$. The parameter values used are (24), $c_1=c_2=1$ and $h=0.1$. The space dimension are 64×64 and we have used periodic boundary conditions.

Defect lattices have in fact been observed in planar EC [26,27] at fairly high frequencies. A theoretical description for these systems by a much more elaborate quantitative theory has been developed recently [20].

V. STATIC CHEVRONS

Here we will relax the condition $c_1=c_2=1$ by reducing c_1 (slightly) below 1. This has no influence on the 1D solutions and their stability with respect to x dependent fluctuations and increases the range of stability with respect to y variations. In fact the critical value of h for the zigzag destabilization of the periodic solutions (dashed line in Fig. 3) is reduced. For example, the period 9.14 is stable in the range

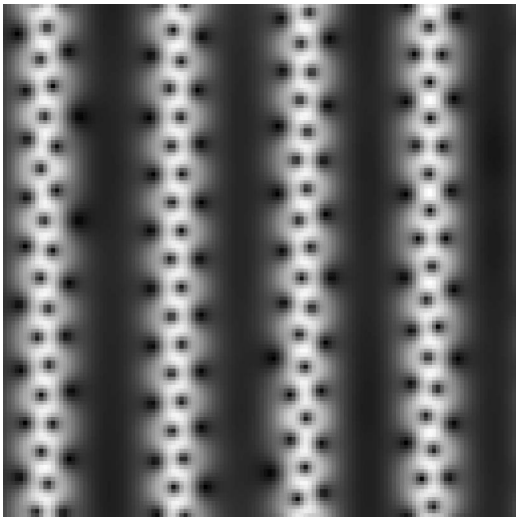

FIG. 11. Static chevron state, gray-scale representation of the field $|A|$. The parameter values used are (24), $c_1=0.9$, $c_2=1$, and $h=0$. The physical dimension is 64×64 and we have used periodic boundary conditions.

$$0.19<h<0.74, \quad \text{when} \quad c_1=0.9, \quad c_2=1, \tag{28}$$

which should be compared to Eq. (27). For values of h beyond the instability the states that we obtain are similar to those found above for $c_1=1$. Namely, we observe states with 2D order close to the instability point (with some hysteresis), which get progressively less ordered as h is decreased. When c_1 is decreased further the stable range of the periodic solutions extends to progressively lower values of h. In fact, for $c_1<0.77$ the 1D solutions with period 9.14 are stable down to $h=0$.

For $h=0$ we obtain a static pattern containing lines (or bands, i.e., multiple lines) of defects along the y direction, which resemble the usual chevron states, except that those are dynamic. In Figs. 11 and 12 such a solution is presented for $c_1=0.9$. The defects (zeros of $|A|$) are located at the dark points in Fig. 11. Within one band, all defects have the same topological charge and this is alternating from band to band. The dark regions between defect bands imply a small value of $|A|$. As one sees from Fig. 12 the field ϕ varies periodically essentially only in x, and thus is very reminiscent of the 1D patterns discussed before. We call these new patterns ''static chevrons.'' They are formed from random initial conditions.

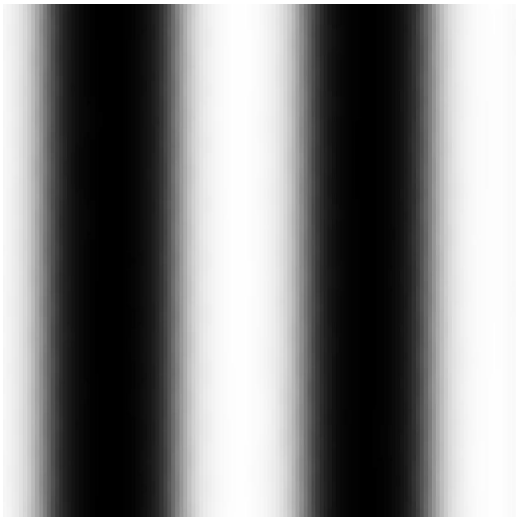

FIG. 12. The field ϕ for the static chevron state of Fig. 11.

The static chevrons persist for small nonzero values of the parameter h. If we let the chevron states be created for $h=0$ and then increase h the static chevrons persist up to $h\leqslant0.015$ for the parameters used here. Increasing h further ($h=0.02$) we observe that more defect bands are created, that is, we have chevrons with a shorter period, but these are now the dynamic chevrons presented previously for $c_1=1$ [17,28]. For even larger values of h one reaches the much less correlated defect chaotic state discussed before. For c_1 closer to 1 the correlations become weaker.

To gain an understanding of static chevrons we first note that the states between the defect bands should be interpreted as (approximately) homogeneous states with nonzero wave number P in the y direction, i.e., with complex amplitude

$$A=A_0e^{\pm iPy}, \tag{29}$$

where the sign in the exponent alternates between neighboring regions and the magnitude of P is related to the number of defects ρ per unit length in one band through the relation

$$\rho=\frac{P}{\pi}. \tag{30}$$

This follows directly from the fact that each defect contributes a phase change of $\pm2\pi$, depending on its topological charge. In the simulations we find that ϕ and P take values close to

$$\phi_A=\pm\frac{1}{\sqrt{1-c_1^2}} \quad \text{and} \quad P_A=c_1\phi_A \tag{31}$$

in the region between the defect bands, while A_0 is small as was already mentioned.

The uniform solutions are described by equating the right-hand sides of Eqs. (7) to zero. The resulting cubic equation for ϕ_0 can be written as

$$(\phi_0-c_2P)^3-2\phi_0(1-c_1c_2)(\phi_0-c_2P)^2 + [(1+c_2^2-2c_1c_2)\phi_0^2-c_2^2](\phi_0-c_2P)+hc_2^2\phi_0=0. \tag{32}$$

In the limit $h\to0$ one of the solutions tends to

$$A_0^2=1-\frac{1+c_2^2-2c_1c_2}{c_2^2}\phi_0^2, \quad \phi_0=Pc_2 \tag{33}$$

and the other two tend to

$$A_0=0, \quad \phi_0=c_1P\pm\sqrt{1-P^2(1-c_1^2)}. \tag{34}$$

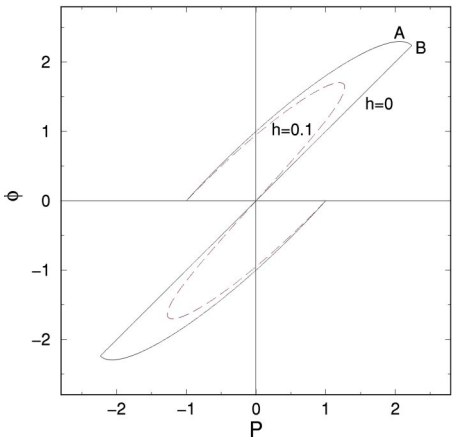

FIG. 13. The solutions of Eq. (32) (with $A_0^2>0$) in the ($P-\phi_0$) plane for two values of the field $h=0$ (solid line) and $h=0.1$ (dashed line). The parameter values are $c_1=0.9, c_2=1$. The point A has coordinates $\phi_A=1/\sqrt{1-c_1^2}, P_A=c_1\phi_A$ and the point B has $\phi_B=c_2/\sqrt{1+c_2^2-2c_1c_2}$, $P_B=\phi_B/c_2$.

Here one has to impose the additional restriction that $\phi_0/(\phi_0-c_2P)>0$, since otherwise A_0^2 is not positive for h slightly away from zero. In Fig. 13 ϕ is sketched for these limiting solutions as a function of P (solid lines). Solution (33) is the continuation of the NRs to nonzero P. Similarly, Eq. (34) represents the continuation of ARs. The two lines join at point B in Fig. 13.

We can now see that the states between the defect bands given in Eq. (31) correspond (approximately) to the continued ARs of Eq. (34) with the *maximal* $|\phi_0|$. Thus the defect bands connect between the two symmetry degenerate versions of this state. A simple stability analysis explains why this state is selected. We write $A=A_0+a$ and $\phi=\phi_0+\varphi$ and linearize Eqs. (3) and (4) in a,φ. For $A_0=0$ the two equations separate and we obtain the following expression for the growth rate of the mode involving a:

$$\tau\sigma=1-s_x^2-s_y^2+2c_1c_2\phi_0s_y-c_2^2\phi_0^2. \tag{35}$$

One easily checks that all states are unstable against fluctuations along y except for state (31), which is marginally stable. The latter is denoted by the letter A in Fig. 13.

The static chevron states that are periodic and describe spatial oscillations between states (31) need not be themselves marginally stable. On the contrary, they are numerically found to be quite robust. This observation is in agreement with the results of Sec. IV A that the 1D periodic states are stable even for parameter values for which the uniform states are unstable.

The effect of the value of c_1 on the chevron states is rather profound. This is seen by the (approximate) relation giving the density of defects in the chevrons, which can be found using Eqs. (30) and (31):

$$\rho=\frac{c_1}{\pi\sqrt{1-c_1^2}}. \tag{36}$$

Thus, as c_1 approaches 1 the defect bands become broader (the separation between defects inside a band is rather independent of parameters). In the limit $c_1\to1$, one expects existence of an infinite lattice of defects with the same polarity, but this is not accessible numerically, and presumably also not experimentally. On the other hand, as c_1 decreases, the number of defects per unit length decreases quickly reaching a situation with a single chain in a band. Decreasing c_1 further one reaches a critical value below which no defects are created. Instead one has the 1D periodic modulations without defects, which are here stable also for $h=0$ (see above).

We have mentioned already that static chevrons persist to slightly nonzero h. In order to understand the defect-free regions for this case we have studied the homogeneous solutions as obtained from Eq. (34). In Fig. 13 we also show ϕ_0 for the case $h=0.1$ (dashed). Analyzing the stability we found that there is a small interval around the states with maximal $|\phi_0|$, which are stable. This shows that the disappearance of static chevrons for increasing h is not a result of the homogeneous regions becoming unstable, but rather the defect bands destabilize, which is also observed in simulations.

VI. CONCLUDING REMARKS

Motivated in particular by experiments in electroconvection in homeotropically aligned nematics [14,15]. We have studied some classes of modulated solutions of the Ginzburg-Landau equation for the complex order parameter A describing the bifurcation to a stationary roll pattern, coupled to a weakly damped (or even undamped) homogeneous mode ϕ describing the orientation of the in-plane director, see Eqs. (1) and (2) (unscaled) or Eqs. (3) and (4) (scaled). The most important parameter h in these equations gives the ratio of the aligning torque on the director over the destabilizing torque of normal rolls. The latter is proportional to the supercriticality parameter ε. Another important parameter ν in the equations characterizes the action of the gradient of the in-plane director on the phase of the rolls, which can be controlled experimentally by varying the frequency. Our study is relevant for $\nu>0$, which is the case in the upper-frequency conduction range and presumably also in the dielectric range [18].

The solutions we considered are characterized by modulations in the direction perpendicular to normal rolls (parallel to the wave vector). There exists a surprisingly rich spectrum of stable solutions of this type even in the range of control parameter, where most homogeneous states have lost stability. The simplest type has only variations in the direction of the wave vector (1D structures). When such variations arise they lead to the creation of defects, except in a small control parameter region, where 2D defect-free modulations may exist metastably. The solutions with defects range from essentially fully spatially ordered defect lattices to defect chaos with various degrees of spatial correlations. Their detailed study appears interesting, but is beyond the scope of this paper. The complexity of the solutions, as well as their dynamics, generally increase with decreasing h. For very small values of h, however, defects show the tendency to order

along chains (or bands) yielding chevron structures. One mechanism for the generation of dynamic chevrons has been related to a Turing instability [27,28]. We have found for $c_1<1$ a new type of fully ordered, static chevrons that appear more related to the 1D structures.

Focusing on the in-plane ($=\hat{c}$) director field, the modulations occur along the direction of prealignment of the in-plane director (from this point of view they give rise to ''bend'' distortions). In fact, there is a long history of observations of such modulated states under an electric field in highly doped MBBA [29–32] and other nematic materials [33,34] at high frequency, often without detectable convection rolls. They come under the name of ''wide domains'' [29,30,33] or ''prechevrons'' [31,32]. Since such structures cannot be explained purely statically, it seems reasonable to assume that they are secondary structures of the type discussed here. The mechanism for the generation of the primary roll pattern, which may not be visible, is presumably different from the usual Carr-Helfrich mechanism. In fact, it was shown that the driving mechanism persisted above the nematic-isotropic transition [32]. Moreover, in Ref. [33] it was shown that a treatment of the bounding plates by tensides led to a considerable increase of the frequency range, where the wide domains appeared. These findings, which are consistent with some old results [35], indicate that an isotropic mechanism with rolls confined to the boundaries is involved.

It was found that even after the wide domains have formed the usual electroconvection would set in at the expected threshold [31,32]. In the dielectric regime this would lead directly to perfectly ordered chevrons that have an appearance like the static chevrons presented above.

While states modulated only along the direction of the wave vector have been observed to some extent, the observation of corresponding two-dimensional modulations without defects is lacking. This may be due to the small parameter range, where such 2D modulations occur and also because of their apparent metastability. An experimental effort in this direction appears interesting. The present results suggest that the objective should be to observe successively the 1D and 2D modulations and the chevron states and to test if they can be related to each other according to the present theory.

Equations (3) and (4) also allow for solutions that are modulated only along the rolls (perpendicular to the prealignment of the in-plane director, giving rise to a ''splay'' distortion). Then the phase of the patterning mode (i.e., the phase of A) comes into play, and the periodic solutions in fact correspond to zigzag patterns. Such states are of relevance for smaller values of ν, in particular for $\nu<0$. Near the zigzag instability of normal rolls, which occurs at $h=1-\nu$, and thus precedes the transition to abnormal rolls for $\nu<0$, the periodic patterns are unstable. For smaller values of h (larger ε) there are various types of periodic patterns. The scenario is enriched by the fact that the usual defects (point dislocations) can extend in the direction perpendicular to the rolls to form phase slip lines [21].

In order to extend the treatment to larger ε one has to use more complicated equations derivable from an extended nonlinear analysis, which includes in particular mean flow. For planar convection in the conduction regime the analysis has been carried out and relevant solutions involving in particular realistic defect lattices have been studied [20]. For the dielectric regime an extended weakly nonlinear study was presented in Ref. [18]. The system appears interesting in view of its parameters $c_1=c_2=\nu=0.98$ calculated under neglect of flexoelectric effects, which are of more relevance in the dielectric regime (note that in Ref. [18] the c_i correspond to our C_i). There is hope to find static chevrons if the aligning torque could be made sufficiently small by applying a destabilizing magnetic field. One might use this technique also in the conduction range, where c_1 is substantially smaller than 1 [20]. However, one may then have to include higher-order terms in Eq. (4).

ACKNOWLEDGMENTS

We wish to thank Á. Buka, N. Éber, B. Dressel, W. Pesch, and A.G. Rossberg for useful discussions. We are grateful to A.G. Rossberg for making available his method and code for identifying defects [36]. Financial support from the European graduate school ''Nonequilibrium Phenomena and Phase Transitions in Complex Systems,'' by DFG under Contract No. KR 690/16-1, and from the TMR program Grant No. ERBFMRXCT960085 funded by EU is gratefully acknowledged.

[1] F. Simoni, in *Nonlinear Optical Properties of Liquid Crystals* (World Scientific, Singapore, 1997); G. Demeter, Phys. Rev. E **61**, 6678 (2000).

[2] T. Börzsönyi, A. Buka, A.P. Krekhov, O.A. Scaldin, and L. Kramer, Phys. Rev. Lett. **84**, 1934 (2000).

[3] M.A. Scherer, G. Ahlers, F. Hörner, and I. Rehberg, Phys. Rev. Lett. **85**, 3754 (2000).

[4] L. Kramer and W. Pesch, in *Physical Properties of Liquid Crystals*, edited by D. A. Dunmur, A. Fukuda, and G. R. Luckhurst (EMIS Datareview Series, IEEE, New York, 2001), Vol. 1.

[5] *Pattern Formation in Liquid Crystals*, edited by Á. Buka and L. Kramer (Springer-Verlag, Berlin, 1995).

[6] H. Richter, A. Buka, and I. Rehberg, in *Spatio-Temporal Patterns in Nonequilibrium Complex Systems*, edited by P. Cladis and P. Palffy-Muhoray (Addison-Wesley, New York, 1994).

[7] H. Richter, A. Buka, and I. Rehberg, Phys. Rev. E **51**, 5886 (1995).

[8] H. Richter, N. Klöpper, A. Hertrich, and A. Buka, Europhys. Lett. **30**, 37 (1995).

[9] Sh. Kai, K. Hayashi, and Y. Hidaka, J. Phys. Chem. **100**, 19 007 (1996); Y. Hidaka, J. Huh, K. Hayashi, M. Tribelsky, and Sh. Kai, J. Phys. Soc. Jpn. **66**, 3329 (1997); Y. Hidaka, J.H. Huh, K. Hayashi, Sh. Kai, and M.I. Tribelsky, Phys. Rev.

E **56**, R6256 (1997).
[10] A. Hertrich, W. Decker, W. Pesch, and L. Kramer, J. Phys. II **2**, 1915 (1992); L. Kramer, A. Hertrich, and W. Pesch, in *Pattern Formation in Complex Dissipative Systems*, edited by Sh. Kai (World Scientific, Singapore, 1992).
[11] A.G. Rossberg, A. Hertrich, L. Kramer, and W. Pesch, Phys. Rev. Lett. **76**, 4729 (1996); A.G. Rossberg and L. Kramer, Phys. Scr., **T67**, 121 (1996).
[12] L. Kramer and W. Pesch, in *Pattern Formation in Liquid Crystals*, edited by A. Buka and L. Kramer (Springer-Verlag, Berlin, 1995).
[13] P. Tóth, Á. Buka, J. Peinke, and L. Kramer, Phys. Rev. E **58**, 1983 (1998).
[14] Á. Buka, P. Tóth, N. Éber, and L. Kramer, Phys. Rep. **337**, 157 (2000).
[15] A.G. Rossberg, N. Eber, A. Buka, and L. Kramer, Phys. Rev. E **61**, R25 (2000); N. Eber, S. Nemeth, A.G. Rossberg, L. Kramer, and Á. Buka, *ibid.* **66**, 036213 (2002).
[16] E. Plaut, W. Decker, A.G. Rossberg, L. Kramer, W. Pesch, A. Belaidi, and R. Ribotta, Phys. Rev. Lett. **79**, 2367 (1997).
[17] A. G. Rossberg, Ph. D. thesis (in English), University of Bayreuth, 1998.
[18] A.G. Rossberg, Phys. Rev. E **62**, 8114 (2000).
[19] L. Kramer, B. Dressel, H. Zhao, and W. Pesch, Mol. Cryst. Liq. Cryst. **364**, 101 (2001).
[20] B. Dressel, Ph. D. thesis, University of Bayreuth 2002; B. Dressel and W. Pesch (private communication).
[21] H. Zhao, Ph. D. thesis (in English), University of Bayreuth, 2000.
[22] P. Coullet, C. Elphick, and D. Repaux, Phys. Rev. Lett. **58**, 431 (1987).
[23] A. Hagberg and E. Meron, Chaos **4**, 477 (1994); A. Hagberg, E. Meron, I. Rubinstein, and B. Zaltzman, Phys. Rev. E **55**, 4450 (1997).
[24] S. Rudroff, H. Zhao, L. Kramer, and I. Rehberg, Phys. Rev. Lett. **81**, 4144 (1998).
[25] H. Zhao and L. Kramer, Phys. Rev. E **62**, 5092 (2000).
[26] S. Nasuno, O. Sasaki, Sh. Kai, and W. Zimmermann, Phys. Rev. A **46**, 4954 (1992).
[27] A. Belaidi, A. Joets, and R. Ribotta (unpublished); A. Belaidi, Ph. D. thesis, Université de Paris-Sud, Orsay, 1998.
[28] A.G. Rossberg and L. Kramer, Physica D **115**, 19 (1998).
[29] A. N. Trufanov, L. M. Blinov, and M. I. Barnik, in *Advances in Liquid Crystal Research and Applications*, edited by L. Bata (Pergamon Press, Oxford, 1980), p. 549.
[30] L. Nasta, L. Lupu, and M. Giurgea, Mol. Cryst. Liq. Cryst. **71**, 65 (1981).
[31] J.-H. Huh, Y. Hidaka, A.G. Rossberg, and S. Kai, Phys. Rev. E **61**, 2769 (2000).
[32] J.-H. Huh, Y. Hidaka, Y. Yusuf, S. Kai, N. Éber, and Á. Buka, Mol. Cryst. Liq. Cryst. **364**, 111 (2001); J. -H. Huh, Y. Yusuf, Y. Hidaka, and S. Kai (unpublished).
[33] W. Weissflog, G. Pelzl, H. Kresse, and D. Demus, Cryst. Res. Technol. **23**, 1259 (1988).
[34] N. Éber, T. Tòth-Katona, Á. Buka (private communication).
[35] R. Ribotta and G. Durand, J. Phys. Colloq. **40**, C3-334 (1979).
[36] Available at http://www.rossberg.net/ag/defects.